Surface Science 606 (2012) L13–L17

Contents lists available at SciVerse ScienceDirect

Surface Science

journal homepage: www.elsevier.com/ locate/susc

Surface Science Letters

Effect of surface groups on the luminescence property of ZnO nanoparticles synthesized by sol–gel route

A. Sharma [a,*], B.P. Singh [a], S. Dhar [a], A. Gondorf [b], M. Spasova [b]

[a] Department of Physics, Indian Institute of Technology Bombay, Powai, Mumbai-400076, Maharashtra, India
[b] Universität Duisburg-Essen, Fakultät für Physik, Experimentalphysik, AGLorke, Lotharstr.1, 47057, Duisburg, Germany

ARTICLE INFO

Article history:
Received 18 July 2011
Accepted 6 September 2011
Available online 14 September 2011

Keywords:
ZnO
Sol–gel
Photoluminescence
Surface groups
Physisorption

ABSTRACT

Structural and optical properties of ZnO nanoparticles of diameter ~5 nm synthesized by a sol–gel route, have been studied using a variety of experimental techniques. The photoluminescence (PL) study carried out on these particles in the atmospheric and vacuum conditions shows a suppression of the defect related green luminescence (GL) band and a simultaneous enhancement of the near-band-edge ultra violet luminescence (UVL) when the surroundings of the nanoparticles are evacuated. This observation clearly suggests that GL is originating from certain groups that are physisorbed on the surface of the nanoparticles. Fourier transform infrared spectroscopy (FTIR) that has also been conducted at the vacuum and atmospheric conditions reveals the presence of the hydroxyl and the acetate groups in these nanoparticle samples. These groups are also found to be removed upon evacuation, suggesting that there is physical adsorption on the surface of the nanoparticles. When the PL spectrum is recorded again at the atmospheric condition, the GL intensity recovers almost up to its original value. Since there are substantial amount of water molecules present in air, which can source the hydroxyl groups, while the acetate groups are not expected to be abundant in air, this finding further suggests that the hydroxyl groups rather than the acetate groups are the likely cause for the GL emission observed in this system.

1. Introduction

ZnO is a promising wide band semiconductor for ultraviolet (UV) and visible light optoelectronics. Because of the band gap tunability and low production cost, ZnO nanoparticles have a lot of potentials for applications in the field of light emitting diodes (LEDs) and laser diodes (LDs). However, their potential for UV devices is impaired because of the reduction of UV luminescence (UVL) yield due to the presence of a large density of unintentional defect states emitting a broad band of green luminescence (GL) [1–3]. The latter, though can be utilized effectively for the visible light optoelectronic devices, the UV devices would require its complete suppression. Both the UV and the visible luminescence can potentially be utilized to fabricate optoelectronic devices using ZnO nanoparticles; a control over their relative intensities is imperative. In order to achieve such a control, the understanding of the origin of the GL emission is foremost important. Even though a large volume of research has been devoted along that direction, the origin of green luminescence still remains controversial. In case of ZnO thin films GL has been assigned to various types of defects such as oxygen vacancies (V_O), oxygen antisites (O_{Zn}) [4–6], Zn vacancies (V_{Zn}) [7] and Zn interstitials (Zn_i) giving rise to red, orange, yellow, and green luminescence [8–10]. Many reports also suggest extrinsic impurities such as Cu to be the likely cause for the origin of green luminescence (GL) band [11,12]. In case of ZnO nanoparticles, GL is often believed to be stemming from the surface [13–15]. However, the precise origin of this feature is yet to be understood. Role of the surface becomes more crucial for the smaller particles as the surface to volume ratio increases with the decrease of the particle size. In order to exploit the advantages of quantum confinement effect, which results in an enhancement of the band gap with the reduction of the particle size, the particle radius has to be comparable or smaller than the excitonic Bohr radius of ZnO that is only ~2.5 nm. Therefore, it is a challenge to enhance both the energy and the relative intensity of the UVL emission with respect to the GL emission at the same time.

Here, we have performed a comparative study of the optical and the structural properties of ZnO nanoparticles before and after their surroundings are evacuated. Our study reveals that certain groups that are physically adsorbed on the surface of the nanoparticles are responsible for the GL emission. The study further suggests that out of the two

* Corresponding author. Tel.: +91 2225764570.
E-mail addresses: archana3@iitb.ac.in (A. Sharma), bhanups@phy.iitb.ac.in (B.P. Singh), dhar@phy.iitb.ac.in (S. Dhar), andreas.gondorf@uni-due.de (A. Gondorf), marina.spasova@uni-due.de (M. Spasova).

0039-6028/$ – see front matter © 2011 Elsevier B.V. All rights reserved.
doi:10.1016/j.susc.2011.09.006

most probable candidates, namely the hydroxyl groups and the acetate acetate groups, the hydroxyl groups are likely to be responsible for the GL emission observed in our ZnO nanoparticle samples.

2. Experimental

ZnO nanoparticles are synthesized by a sol–gel technique [16]. In this process Zn-acetate powder is used as Zn precursor. This powder is mixed to obtain 0.16 mM solution in 100 ml ethanol at room temperature. The solution initially forms a white color suspension. The mixture is then transferred into a distillation apparatus and boiled under vigorous stirring at 70 °C for 1 hour (Sol. A). 7 mM of $LiOH.2H_2O$ powder is mixed in 50 ml of ethanol. The suspension is kept in an ultrasonic bath at room temperature for 20 minutes to obtain a homogeneous solution (Sol. B). The hydroxide containing solution (Sol. B) is added drop wise at a rate of 5 ml/min to the Sol. A under vigorous stirring maintained at 70 °C and then placed in an ultrasonic bath for 1 hour at room temperature. In order to separate ZnO nanoparticles from the solution, the following decantation procedure is implied. Hexane is added to the mixture until a turbid solution is formed. Hexane dissolves all the by-products of the process and ZnO nanoparticles segregate from the solution as precipitate. The precipitate is then collected and redissolved in ethanol. Hexane is again added to the solution. This process is repeated for several times. Finally, the precipitate is dried in air and ZnO nanoparticles are collected as powder. The structural properties of the nanoparticles are investigated by high resolution transmission electron microscopy (HRTEM), X-ray photoemission spectroscopy (XPS), X-ray diffraction (XRD), Fourier transform infrared absorption (FTIR) spectroscopy and Raman Spectroscopy. Nanoparticles are redissolved in methanol and casted on Cu-grids for HRTEM study. Powder samples are used for XRD, Raman and XPS studies. Optical properties are investigated through photoluminescence (PL) and absorption spectroscopy. Colloidal suspension of nanoparticles in methanol is used for absorption studies. Nanoparticles are casted on cleaned Si substrates for PL studies. He–Cd laser source of wavelength $\lambda = 325$ nm and power of 25 mW was used for the excitation. An Acton monochromator attached with a CCD camera was used to obtain the spectra. PL measurements are performed at room temperature while keeping the sample either in the vacuum or in the atmospheric conditions. In the vacuum condition, the pressure inside the chamber was recorded to be approximately 5×10^{-4} Torr. FTIR studies are also carried out both in the vacuum and the atmospheric conditions. In the atmospheric conditions, FTIR studies are conducted on compressed pellets prepared by mixing powder samples with potassium bromide (KBr). While in case of our vacuum FTIR studies, powder samples of ZnO nanoparticles are kept in an ultra high vacuum (UHV) chamber during the measurement. Raman spectroscopy was performed using Horiba Jobin Yvon HR640, using 514 nm Ar ion laser as the excitation source.

3. Results and discussion

3.1. Structural properties

Fig. 1(a) shows the HRTEM image of a ZnO nanoparticle. The diameter of the particle visible in this image is ~5.5 nm. Fast Fourier transform (FFT) of the image shown in the inset of Fig. 1(a) confirms the formation of ZnO in hexagonal wurtzite structure. The lattice parameters calculated from the FFT pattern matches very well with that of ZnO. Fig. 1(b) shows a TEM image of these ZnO nanoparticles. The histogram plot describing the particle size distribution is shown in the inset. This distribution is obtained by analyzing the size of about 300 particles from several such TEM images.

Fig. 2 shows the absorption spectra taken for suspended ZnO nanoparticles. The profile resembles the absorption spectra typically found for ZnO nanoparticles suspended in alcohol solutions featuring a sharp on-set followed by a peak at higher energy. The energy E ($\lambda_{1/2}$) is the energy position at which the absorption is half of its peak value, is usually considered as the average band-gap of the nanoparticles. E ($\lambda_{1/2}$) for our ZnO nanoparticles (≈3.65 eV) is found to be higher than the band gap (E_g) energy (≈3.32 eV) of bulk ZnO that confirms the quantum confinement effect. The average particle diameter can be obtained from E ($\lambda_{1/2}$) using tight binding model (TBM) [17].

$$\Delta E_g = 100/\left(18.1d^2 + 14.4d - 0.8\right) \quad (1)$$

where, $\Delta E_g = E(\lambda_{1/2}) - E_g$ and d is the mean diameter for the nanoparticles. In this case d is estimated to be ~5.2 nm, which matches well with the mean diameter obtained from the particle size distribution shown in the inset of Fig. 1(b).

Fig. 3 represents the wide angle X-ray diffraction (XRD) profiles for the ZnO nanoparticles. All the peaks can easily be identified as (100), (002), (101), (102), (110), (103) and (112) reflections associated with wurtzite phase of ZnO. No additional feature related to impurity phase can be seen in the XRD profile. Average diameter of the nanoparticles is estimated to be 6 nm from the full width at the half maximum (FWHM) of (101) peak using Debye-Scherrer formula [18]. Both a and c-lattice constants are estimated to be 3.23 and 5.20 Å, respectively from these peak positions. Interestingly, both the parameters

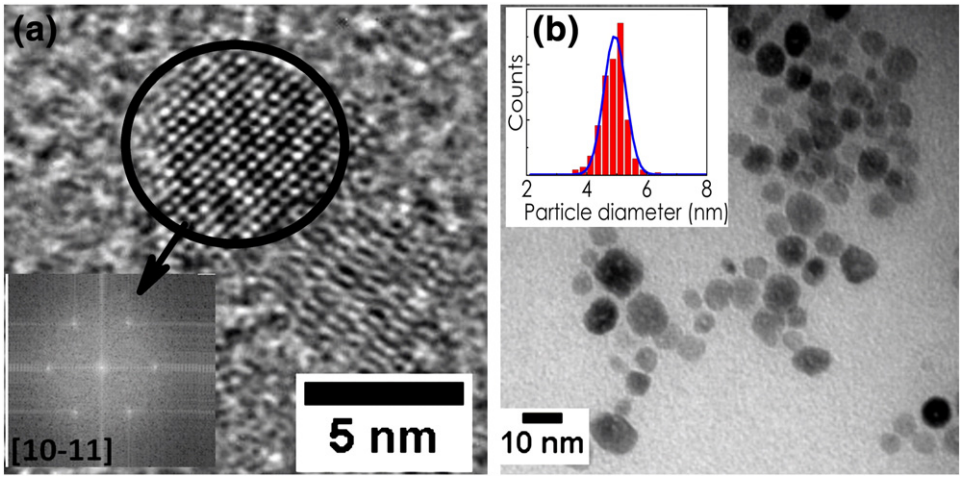

Fig. 1. (a). HRTEM image of a ZnO nanoparticle. Inset shows the Fast Fourier Transform (FFT) of the image. (b) TEM overview image of the ZnO nanoparticles. Inset shows the particle size distribution. Bar shows the number of particles and the thick line is the gaussian fit used to calculate mean diameter of the nanoparticle.

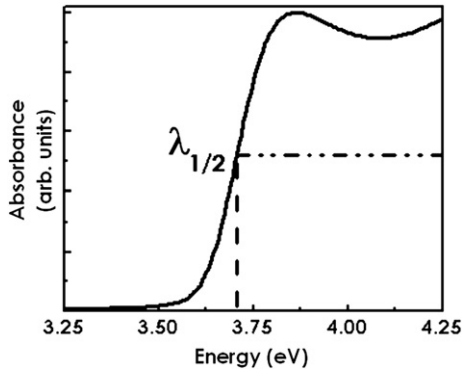

Fig. 2. Absorption profile of ZnO nanoparticles suspended in ethanol medium.

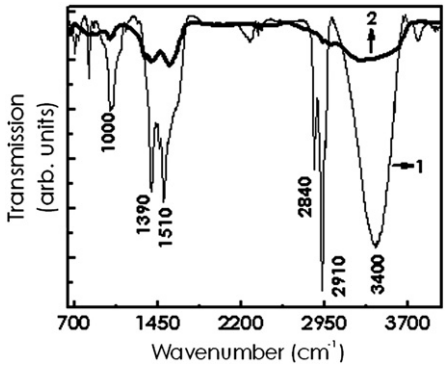

Fig. 4. FTIR spectra of ZnO nanoparticles recorded in the atmospheric (curve 1) and the vacuum conditions (curve 2).

are found to be little less than those obtained for bulk ZnO samples ($a = 3.25$ Å and $c = 5.21$ Å) [19].

Fig. 4 compares the FTIR spectra recorded for samples under the atmospheric and vacuum conditions. Clearly, certain absorption features are visible in both the conditions. For example, the feature appearing between 1400 and 1600 cm^{-1}, which comprises of several peaks, are attributed to the stretching modes (symmetric and asymmetric) of the acetate group (-COOH) [20]. These groups are believed to be adsorbed on the surface of the nanoparticles during the synthesis process. The absorption peak appearing at 1000 cm^{-1} is due to C═O deformation mode of the acetate groups. Few narrow peaks appearing around 2830 cm^{-1} and 2920 cm^{-1} due to C–H bond can also be seen [21]. The broad feature appearing around 3400 cm^{-1} is resulting from the hydroxyl (–OH) group [20, 21]. It is noticeable that the intensity of all these features decreases upon evacuation. Since the same amount of material is used for the FTIR studies carried out both in the vacuum and the atmospheric conditions, our FTIR results indicate that the density of the hydroxyl and the acetate groups decreases when the surroundings of the nanoparticles are evacuated, which further implies that these groups are physisorbed on the surface (but not chemically bonded) of the ZnO nanoparticles such that they can be removed upon evacuation.

Fig. 5 represents the Raman spectra for the ZnO nanoparticles. Raman features in ZnO powder are ascribed to Raman active modes of the ZnO wurtzite crystal [22]. Wurtzite-type ZnO belongs to the space group $P_6 3mc$, with two formula units per primitive cell. The zone center optical phonons can be classified according to the following irreducible representation: $\Gamma_{opt} = A_1 + E_1 + 2E_2 + 2B_1$, where B_1 modes are silent, A_1 and E_1 are polar modes, both Raman and infrared active, while E_2 modes (E_2 low and E_2 high) are non polar and Raman active only. The E_2 (high) Raman mode observed at 437 cm^{-1} is dominantly assigned to the oxygen vibration [22, 23]. The E_1 (LO) mode present at 578 cm^{-1} usually originates from second-order Raman scattering. Although the presence of impurities and/or defects can also influence these modes, the E_1 (LO) mode is more strongly affected by these effects [23]. The peak at 332 cm^{-1} is assigned to the second-order Raman process [22]. Other vibrational peaks, which originated from acetate group are assigned in Fig. 5. The acetate ligand can be in the forms of free zinc acetate or potassium acetate (KAc). Some of this ligand is also believed to be attached to the ZnO surfaces. As the vibration frequencies of the functional groups are sensitive to the chemical environment, the Raman spectra can help in identifying the chemical forms of the acetate ligand. However, the C-O stretch and O-C-O bend modes are much more sensitive to the surrounding environment. The C-O stretch of acetate is red-shifted by 5 cm^{-1} compared to that of KAc and 24 cm^{-1} to free zinc acetate [24]. This result shows the absence of free acetate group or potassium acetate present in the powder. Instead, they are bound to ZnO surfaces as has been clearly observed in our FTIR results [25].

XPS is used to investigate the chemical composition of ZnO nanoparticles. The survey scan (not shown here) of the ZnO nanoparticles shows the presence of different peaks that can be attributed to Zn, O, and C elements. No impure feature is observed in these samples. Fig. 6 shows (a) O 1s core level (b) $Zn2p_{3/2}$ core level XPS spectra for ZnO nanoparticles. It has to be clearly mentioned that binding energies are calibrated by taking the carbon C1s peak (285.0 eV) as reference in these spectra. In the XPS spectra, the open circles denote the experimental data, thick solid line represents the fitted curve and the deconvoluted individual peaks are depicted by thin solid lines. In Fig. 6(a), the deconvolutions show the presence of five different O1s peaks in the ZnO nanoparticles. The peak located at 529.8 eV (curve 1) is attributed to the H bonds attached to the ZnO surface [26]. The peak centered at 531.2 eV (curve 2) is associated to the O_2^- ions in the wurtzite structure surrounded by the Zn atoms [27]. The peaks at 531.96 (curve 3) and 532.67 eV (curve 4) are attributed to the presence of –OH bonds attached to Zn ions on the surface of ZnO nanoparticles [28]. The

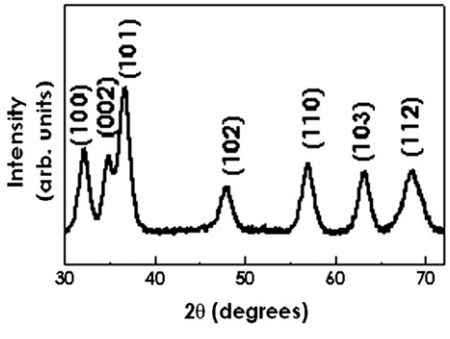

Fig. 3. XRD patterns of ZnO powder nanoparticles showing all the reflections corresponding to wurtzite phase.

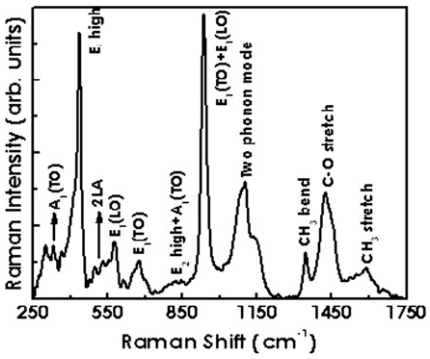

Fig. 5. Raman spectra of ZnO nanoparticles.

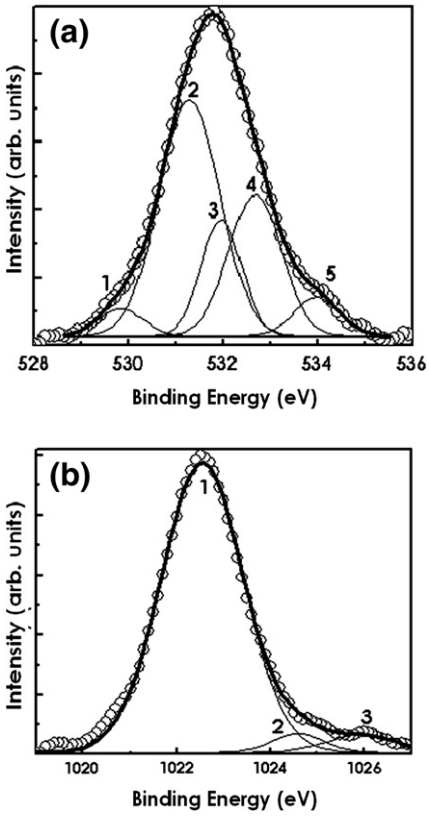

Fig. 6. (a) O1s XPS spectra (b) $Zn2p_{3/2}$ XPS spectra of ZnO nanoparticles. The open symbols in the figure represent the experimental data, thick solid line represents the fitted data and thin solid lines represent the components used to deconvolute the experimental peak.

binding energy peak at 533.98 eV (curve 5) can be ascribed to the certain oxygen containing groups adsorbed at the surface such as $-COO$, O_2 or H_2O [29]. The deconvolutions of the XPS spectra for core level Zn $2p_{3/2}$ of ZnO nanoparticles are represented in Fig. 6(b). A good fit to the experimental data could be obtained only when the data is deconvoluted with three Gaussians indicating the existence of three zinc species in ZnO nanoparticles. Shift in the binding energy towards higher value from 1021 eV rules out the presence of elemental Zn in the ZnO nanoparticles. The observed peak at the binding energy of 1022.56 eV (curve 1) is associated to Zn species in ZnO. The other peak present at higher binding energy of 1024.6 eV (curve 2) corresponds to the hydroxyl groups attached to Zn ions on the surface of the nanoparticles. The peak present at 1025.94 eV (curve 3) could be present due to the formation of zinc oxy-hydroxide compound (ZnO–(OH)) [29–32]. Hence, our XPS result also confirms the presence of many oxygen species attached to the surface of ZnO nanoparticles.

3.2. Optical properties

Fig. 7 shows room temperature PL spectra recorded at the atmospheric condition and at the vacuum. The figure compares the room temperature PL spectra obtained in the atmospheric (thin solid line) and the vacuum (dashed line) conditions for ZnO nanoparticle sample. The curve 3 shown in the form of thick solid line represents the PL spectra when the experiment is performed again in the atmospheric condition. In all cases, an ultra violet luminescence (UVL) band centered at 3.3 eV, resulting from the transition between the conduction and the valance band states can be seen. In addition to that, a broad green luminescence (GL) band is also observed. The GL emission is centered at 2.09 eV for PL performed under atmospheric condition. The GL intensity dominates the UVL intensity when the PL spectra are obtained in the

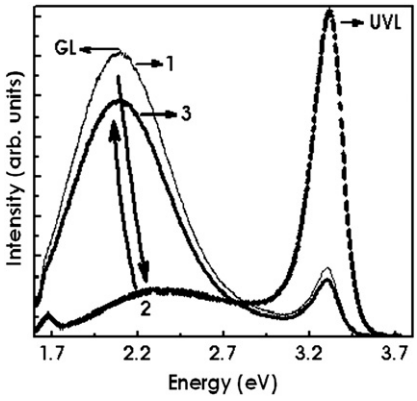

Fig. 7. PL spectra for ZnO nanoparticles in the atmosphere (thin solid line [1]), in vacuum (dashed solid line [2]) and in ambient condition again (thick solid line [3]). The arrows are representing the sequence of the experiments.

atmospheric conditions. On the other hand, the GL emission intensity is much less than that of the UVL emission in vacuum. Note that the green luminescence peak position is slightly blue shifted to 2.35 eV when PL is performed under vacuum condition. This finding clearly suggests that the GL emission must be linked to certain groups which are present on the surface of the nanoparticles in a way that they can be easily removed by evacuation. It is also clear from our FTIR study that hydroxyl and the acetate groups can be easily removed from the surface of the nanoparticles upon evacuation. This indicates that either the hydroxyl or the acetate groups or both are responsible for the GL emission. However, it has to be noted that when the PL spectrum is recorded again at the atmospheric condition, the GL intensity recovers almost up to its original value. This observation suggests that the hydroxyl groups rather than the acetate groups are the likely cause for the GL emission observed in this system because there are plentiful of water molecules in air, which can source the hydroxyl groups. While, the acetate groups are not expected to be abundant in air. The results of Fig. 7 also show that the GL band is not only suppressed but also blue shifted to 2.35 eV under the vacuum condition, which suggests that the origin of GL in the vacuum condition may not be the hydroxyl groups. Here, the native defects such as Zn interstitial or oxygen vacancies could be the possible reason for the residual GL emission. We believe that the GL emission peaking at 2.09 eV, which is observed when the PL is performed under the atmospheric condition, is originating from the hydroxyl groups attached to the ZnO nanoparticles. When these groups are removed upon evacuation, the blue shifted GL band (peaking at 2.35 eV) is most likely resulting from certain native defects or groups, which are chemically bonded to the surface of the nanoparticles and therefore difficult to be removed upon evacuation. It should be noted that our experimental observations show that the presence of surface complexes seems to have a more pronounced effect on the origin of green luminescence from the Photoluminescence studies.

4. Conclusions

We have done a comparative study of the structural and optical properties of ZnO nanoparticles of diameter ~5 nm synthesized by a sol–gel technique. The optical studies have been performed in the atmospheric and vacuum conditions. Our study reveals that certain chemical species, which are physically adsorbed (but not chemically bonded) at the surface of the nanoparticles, are responsible for the GL emission. The study also indicates that the hydroxyl groups are the likely candidate, responsible for the GL emission observed in this system.

Acknowledgment

We would like to acknowledge Nanoelectronics Centre, Electrical Engineering department, IIT—Bombay and Department of Science and Technology (DST) for financial support.

References

[1] D.G. Thomas, J. Phys. Chem. Solids 15 (1960) 86.
[2] A. Tsukazaki, M. Kubota, A. Ohtomo, T. Onuma, K. Ohtani, H. Ohno, S. F. Chichibu, M. Kawasaki, Jpn. J. Appl. Phys., Part 2 44 (2005) L643.
[3] X. Peng, L. Manna, W. Yang, J. Wickham, E. Scher, A. Kadavanich, A.P. Alivisatos, Nature 404 (2000) 59.
[4] F.H. Leiter, H. Alves, D. Pfisterer, N.G. Romanov, D.M. Hofmann, B.K. Meyer, Physica B 201 (2003) 340.
[5] K. Vanheusden, C.H. Seager, W.L. Warren, D.R. Tallant, J.A. Voigt, Appl. Phys. Lett. 68 (1995) 403.
[6] B. Lin, Z. Fu, Y. Jia, Appl. Phys. Lett. 79 (2001) 943.
[7] Q.X. Zhao, P. Klason, M. Willander, H.M. Zhong, W. Lu, J.H. Yang, Appl. Phys. Lett. 87 (2005) 211912.
[8] A.F. Kohan, G. Ceder, D. Morgan, C.G. Van de Walle, Phys. Rev. B 61 (2000) 15019.
[9] N.Y. Garces, L. Wang, L. Bai, N.C. Giles, L.E. Halliburton, G. Cantwell, Appl. Phys. Lett. 81 (2002) 622.
[10] M.A. Reshchikova, H. Morkoc, B. Nemeth, J. Nause, J. Xie, B. Hertog, A. Osinsky, Physica B 401 (2007) 358.
[11] N.Y. Garces, L. Wang, L. Bai, N.C. Giles, L.E. Halliburton, G. Cantwell, Appl. Phys. Lett. 81 (2002) 622.
[12] M.A. Reshchikov, V. Avrutin, N. Izyumskaya, R. Shimada, H. Morkoç, S.W. Novak, J. Vac. Sci. Technol., B 27 (2009) 1749.
[13] H. Zhou, H. Alves, D.K. Hoffmann, W. Kriegseis, B.K. Meyer, G. Kaczmaczyk, A. Hoffmann, Appl. Phys. Lett. 80 (2002) 210.
[14] P.K. Sharma, A.V. Pandey, G. Zolnierkiewicz, N. Guskos, C. Rudowicz, J. Appl. Phys. 106 (2009) 094314.
[15] G. Xiong, U. Pal, J.G. Serrano, K.B. Ucer, R.T. Williams, Phys. Status Solidi C 3 (2006) 3577.
[16] Eric A. Meulenkamp, J. Phys. Chem. B 102 (1998) 5566.
[17] S. Sapra, D.D. Sharma, Phys. Rev. B 69 (2004) 125304.
[18] B. D. Cullity, Elements of X- ray Diffraction, Addison- Wesley Publication Ltd, 1956.
[19] A.A. Dakhel, M. El-Hilo, J. Appl. Phys. 107 (2010) 123905.
[20] G. Xiong, U. Pal, J.G. Serrano, J. Appl. Phys. 101 (2007) 024317.
[21] A.E. Jiménéz-González, J.A. Soto Urueta, R. Su´ arez-Parra, J. Cryst. Growth 192 (1998) 430.
[22] M. Šćepanovic, M. Grujić-Brojčin, K. Vojisavljević, S. Bernik, T. Srećković, J. Raman Spectrosc. 41 (2010) 914.
[23] K.A. Alim, V.A. Fonoberov, M. Shamsa, A.A. Balandin, J. Appl. Phys. 97 (2005) 124313.
[24] K. Nakamoto, Infrared and Raman Spectra of Inorganic an Coordination Compounds, fourth ed. Wiley, New York, 1986.
[25] R.D. Yang, S. Tripathy, Y. Li, H. –J. Sue, Chem. Phys. Lett. 411 (2005) 150.
[26] L.L. Yang, Q.X. Zhao, M. Willander, X.J. Liu, M. Fahlman, J.H. Yang, Appl. Surf. Sci. 256 (2010) 3592.
[27] Ton-That Cuong, Matthew R. Phillips, Foley Matthew, Steve J. Moody, Anton P.J. Stampfl, Appl. Phys. Lett. 92 (2008) 261916.
[28] E. De la Rosa, S. Sepulveda-Guzman, B. Reeja-Jayan, A. Torres, P. Salas, N. Elizondo, M.J. Yacaman, J. Phys. Chem. C 111 (2007) 8489.
[29] N.S. Ramgir, D.J. Late, A.B. Bhise, M.A. More, I.S. Mulla, D.S. Joag, K. Vijayamohanan, J. Phys. Chem. B 110 (2006) 18236.
[30] B.V. Crist, Handbooks of Monochromatic XPS Spectra, Vol. 2: Commercially Pure Binary Oxides, XPS International, Inc, 1999, p. 820.
[31] R. Umebayashi, N. Akao, N. Hara, K. Sugimoto, J. Electrochem. Soc. 150 (2003) B295.
[32] C. Pettenkofer, U. Meier, Appl. Surf. Sci. 252 (2005) 1139.